Polymer Journal (2013) 45, 3–9

www.nature.com/pj

FOCUS REVIEW

Small angle X-ray scattering studies of nanocellular and nanoporous structures

Hideaki Yokoyama

Recently, closed cellular and open porous structures on the nanometer scale have been attracting much attention. Our group has developed a novel method for producing such nanocellular and nanoporous structures using a block copolymer as a template and supercritical carbon dioxide. Small angle X-ray scattering (SAXS) has an important role in characterizing nanocells and nanopores. In particular, grazing incidence SAXS reveals embedded nanocellular and nanoporous structures in thin films. In addition, SAXS can be used for *in situ* measurements to study the process of nanocellular and nanoporous formation in supercritical carbon dioxide. In this focused review, our recent progress on nanocellular and nanoporous fabrication and the use of SAXS techniques to characterize such structures will be presented.
Polymer Journal (2013) **45,** 3–9; doi:10.1038/pj.2012.205; published online 21 November 2012

Keywords: carbon dioxide; GISAXS; *in situ* SAXS; nanocell; nanopore; SAXS; thin film

INTRODUCTION

Nanoscopic structures on the order of nanometers have been attracting an increasing attention. In particular, materials with nanoscopic closed cells (nanocells) and open pores (nanopores) represent a new class of materials that significantly differ from conventional micro- and macrocellular and porous materials. Nanoporous materials have been widely studied for applications involving the separation of molecules (such as proteins), catalysis and ultralow dielectric devices.[1–4] Nanoporous inorganic materials are more established than organic nanocellular and nanoporous materials. The development of inorganic porous materials involves template synthesis using the self-assembly of lyotropic liquid crystals.[5–11] Because inorganic solids are thermally and mechanically robust, lyotropic liquid crystals, which are generally organic surfactants, can be easily removed by heating and oxidation.

However, organic nanoporous and nanocellular materials are far less developed due to their poor thermal and mechanical stability. Among these organic materials, polymeric nanoporous and nanocellular materials have been fabricated using different approaches. The first fabrication of nanoporous polymeric materials was demonstrated by Lee *et al.*[12] They used ordered block copolymers containing a polyisoprene block, which was decomposed by ozone to provide nanopores on the size of the cylindrical polyisoprene domain. The typical pore size was decreased to 25 nm, and the surface area was increased to 50 $m^2 g^{-1}$. The fundamental idea of this decomposition method is that dispersed domains can be selectively removed while continuous matrix domains remain intact. This decomposition method using ordered block copolymers has been further developed by other researchers.[13–16] However, in such a decomposition method, the decomposed fragments need a path to the exterior of the specimen. Therefore, application of the decomposition method is limited to open porous structures and to relatively small specimens.

In addition to the previous decomposition method, selective swelling of block copolymers with supercritical carbon dioxide followed by depressurization has been proven effective in nanocellular and nanoporous fabrication.[17–27] Supercritical fluids selectively swell particular nanodomains and are then removed by depressurization at the end of the process to produce nanocellular and nanoporous structures. In general, closed nanocellular structures cannot be produced using this decomposition method because the decomposed fragments are easily trapped; however, using this method with a supercritical fluid can produce closed nanocells due to the high mobility of supercritical carbon dioxide even in glassy polymeric materials.

The emergence of a variety of nanocellular and nanoporous materials requires analytical tools that can probe nanoscale structures. Analysis of these nanocellular and nanoporous structures is often performed using electron microscopy; however, electron microscopy tends to be qualitative and does not measure the statistically averaged characteristics of the structures. To compensate for this drawback, small angle X-ray scattering (SAXS) techniques are often used to investigate such structures. Conventional transmission SAXS can be used for bulk specimens; however, nanocellular and nanoporous structures are often introduced in thin films, which cannot be measured using transmission SAXS. Grazing incidence SAXS (GISAXS) has an important role in studying nanocellular and

Department of Advanced Materials Science, Graduate School of Frontier Sciences, The University of Tokyo, Chiba, Japan
Correspondence: Professor H Yokoyama, Department of Advanced Materials Science, Graduate School of Frontier Sciences, The University of Tokyo, 603 Transdisciplinary Sciences Bldg, 5-1-5 Kashiwa-no-ha, Kashiwa, Chiba 277-8561, Japan.
E-mail: yokoyama@molle.k.u-tokyo.ac.jp
Received 2 September 2012; revised 3 October 2012; accepted 3 October 2012; published online 21 November 2012

nanoporous thin films on solid substrates. In addition, when nanostructures are embedded, SAXS is one of the few techniques to be used in their analysis. The swollen structures of block copolymers in supercritical carbon dioxide, which are closely related to the final nanocellular and nanoporous structures, are typical examples of embedded nanostructures. *In situ* analysis of swollen block copolymers in compressed fluid can only be achieved using a high-pressure vessel with windows that X-rays can pass through and a bright X-ray beam from synchrotron radiation.

In this focused review, I present our recent progress on the fabrication of nanocellular and nanoporous polymeric materials using block copolymers and supercritical carbon dioxide, and I present the effective uses of X-ray scattering techniques to reveal the structures of such materials.

NANOPOROUS AND NANOCELLULAR FABRICATION USING A BLOCK COPOLYMER AS A TEMPLATE WITH SUPERCRITICAL FLUIDS

Because fluoropolymers or polysilicones (CO_2-philic polymers) have a strong affinity for CO_2, when block copolymers consisting of CO_2-philic and non-CO_2-philic blocks are used, the CO_2-philic domains preferentially swell in CO_2. Consequently, the effective volume fraction of the CO_2-philic block domains significantly increases by selective swelling with CO_2, and thus a 'pressure-induced' order-to-order transition (OOT) may occur. Such selectivity of CO_2 toward CO_2-philic block domains was also utilized for the fabrication of nanocellular and nanoporous structures by removing CO_2 from the swollen block copolymers. Our previous studies have demonstrated the fabrication of closed nanocells from spheres[17–21,25,27] and of stacked nanosheets (lamellae) from cylinders.[22] The high diffusivity, low interfacial tension and excellent surface wettability of CO_2 help to deliver CO_2 into polymers.

However, when the CO_2 pressure is reduced, either macroscopic foam appears[20] or the swollen block copolymers simply shrink back and the nanocells or nanopores are lost. It was found that freezing the swollen block copolymer before decreasing the pressure is essential for converting the swollen nanodomains into nanocells or nanopores.[25] We introduced a temperature quench step before decreasing the pressure so that the surrounding continuous matrix becomes glassy and fixes the structure while a significant amount of CO_2 remains in the CO_2-philic domains.

Although the successful fabrication of nanocells and nanopores can be confirmed using microscopy such as scanning electron microscopy, scattering techniques are also used for the accurate and statistical measurement of the sizes of the nanocells and nanopores. SAXS profiles from nanocellular monoliths are reproduced in Figure 1a.[19] For this particular example, poly(styrene-*b*-perfluorooctylethyl methacrylate) (PS-PFMA) was used as the block copolymer template. PFMA and PS blocks work as CO_2-philic and non-CO_2-philic blocks, respectively. With increasing CO_2 pressure, and hence an increasing degree of swelling during the CO_2 process, the Bragg peaks of the resultant nanocellular structure shift to lower q, indicating that the distances between the nanocells increase with increasing CO_2 process pressure. This is reasonably well supported by the schematic in Figure 1b, in which CO_2-philic spherical nanodomains were highly swollen with CO_2 during the process and converted to nanocells after depressurization. The nanocells were expected to be surrounded by CO_2-philic block domains in a matrix of non-CO_2-philic domains according to the proposed mechanism of nanocellular formation. However, neither scanning electron microscopy nor SAXS provide direct evidence of a CO_2-philic layer surrounding the empty

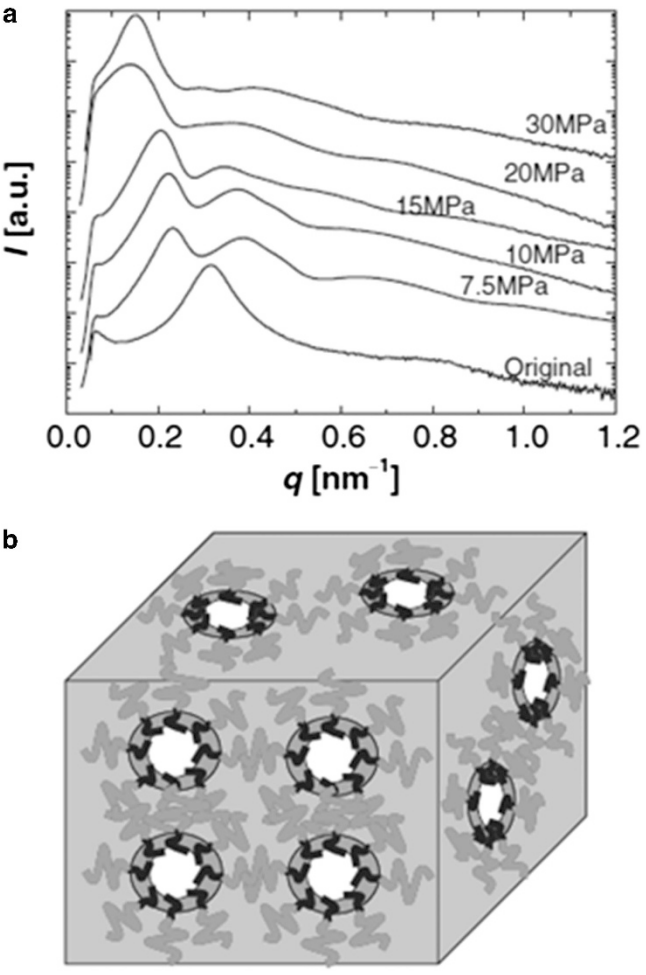

Figure 1 Structures of nanocells: SAXS profiles (**a**) from a bulky nanocellular specimen formed at various process pressures, and the schematic illustration (**b**) of the expected structure, where empty nanocells are surrounded by CO_2-philic block domains. Reproduced from Yokoyama *et al.*[19] with permission.

core. The form factors in the SAXS profiles may contain the structural information for each cell consisting of air, a CO_2-philic block and a non-CO_2-philic block; however, it is difficult to extract the form factor of the nanocells from the SAXS patterns primarily due to interference with the Bragg peaks from the lattice of ordered nanocells. If the form factors of each cell can be isolated from the SAXS profile, we should be able to fit the form factor of a core-shell model with three components, such as air, a CO_2-philic block and a non-CO_2-philic block. I will present an effective method for aligning spherical nanocells in a single layer using thin film confinement, and I will use the GISAXS technique in the following section.[21]

GISAXS FOR NANOCELLULAR AND NANOPOROUS THIN FILMS

The analysis of nanostructures in thin film is increasingly important with advances in nanotechnology. In particular, scattering methods that can be applied to thin films and embedded nanostructures are of great interest. GISAXS has been known to be one of the few useful methods for investigating embedded nanostructures in thin films supported on substrates.[28–45]

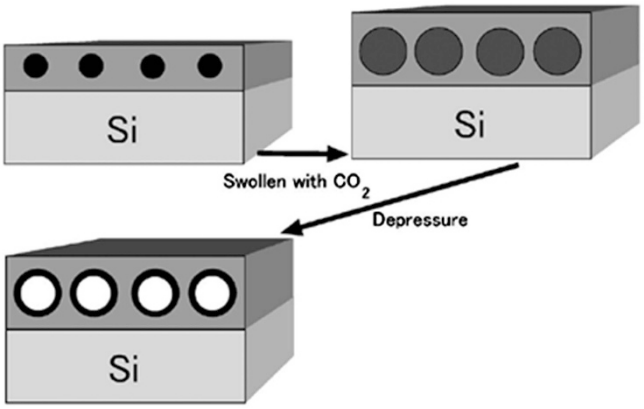

Figure 2 Schematic of the fabrication of nanocells using a block copolymer template and the CO_2 process. CO_2-philic block domains (shown as black) are swollen (dark gray) with CO_2 under CO_2 pressure. The temperature is quenched to 0 °C to freeze the non-CO_2-philic block domains (light gray). After depressurization, the empty cells (white) are introduced into the CO_2-philic block domains. Reproduced from Yokoyama *et al.*[21] with permission.

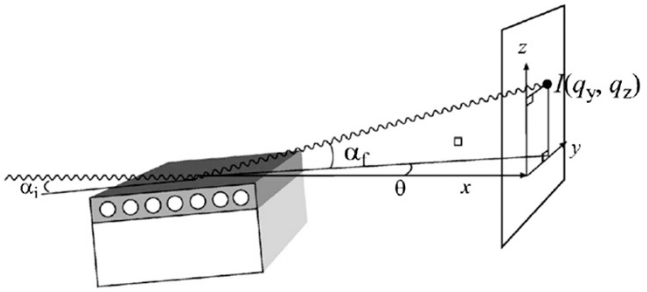

Figure 3 Schematic of the GISAXS geometry. *x* is defined as the direction of the X-ray beam. *y* and *z* are the horizontal and vertical directions. Reproduced from Yokoyama *et al.*[21] with permission.

The presence of the surface and interface has considerable effects on the morphologies of block copolymers. Spherical nanodomains of block copolymers in thin films tend to form a hexagonally ordered array in the plane of the thin films; therefore, a single layer of nanocells ordered in a hexagonal lattice is available through the supercritical carbon dioxide process.[17,18,21] Such a highly ordered structure makes further detailed analysis of the nanocellular structure feasible. We prepared nanocellular thin films using a block copolymer template with carbon dioxide, as shown in Figure 2.

We reported a high throughput destructive method using reactive ion etching to remove the surface covering layer followed by scanning electron microscopy and atomic force microscopy.[17,18] However, such analyses cannot accurately determine the sizes of cells, and a nondestructive quantitative method to analyze the size, shape and spacing of nanocells is desired. In our previous report,[21,22] nanocellular thin films were analyzed by GISAXS. The GISAXS measurement is summarized briefly. A thin film supported on a substrate was placed on a computer-controlled gonio stage. An X-ray beam was guided in at a shallow incident angle, then reflected and scattered by the thin film on the substrate. The geometry of the GISAXS experiment is shown in Figure 3. While diffuse reflectivity is limited to the plane given by the incident beam and the surface normal, which is the x-z plane in Figure 3, GISAXS detects scattering from the surface in all directions. Therefore, GISAXS can probe lateral and vertical structures over a much wider range.

An example of a GISAXS pattern from the nanocellular films at an incident angle of 0.15° is shown in Figure 4a. For the nanocellular thin film, PS-PFMA was used as the block copolymer template, and the nanocells were introduced using supercritical carbon dioxide, as described in the previous section. PFMA and PS blocks work as CO_2-philic and non-CO_2-philic blocks, respectively. This incident angle is above the critical angle of the porous polymer but below the critical angle of silicon. Similar to diffuse reflectivity, GISAXS shows the horizontally extending Yoneda wings at the critical angles of the sample and substrate.[29,46,47] Bragg peaks appear only on the Yoneda wings, indicating that the ordering of the spherical nanocells is restricted in the plane, and hence, the cells form a single layer in the film. In addition to the intense first-order peaks, the higher order peaks are found on the Yoneda wings in Figure 4a. The peak positions

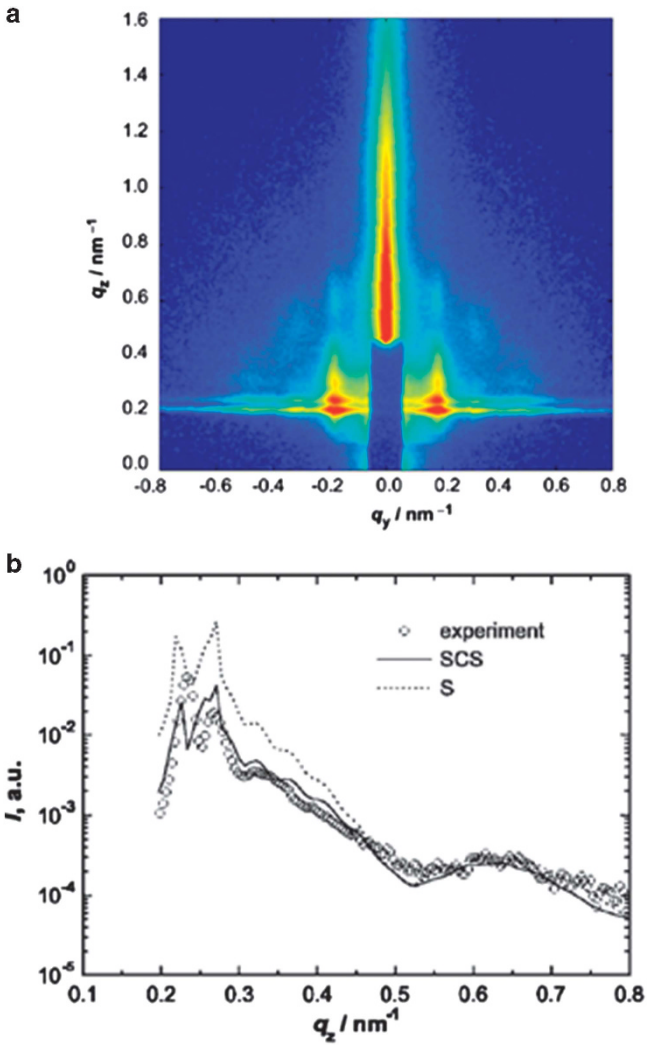

Figure 4 (**a**) An example of a GISAXS pattern from nanocellular block copolymer thin films on a silicon substrate. The horizontal intense streak is called a Yoneda wing (peak). An incident angle of 0.15° was chosen. The intensity increases from blue to red using a logarithmic scale. (**b**) Intensities vs q_z of the nanocellular thin film at the peak q_y. The solid and dotted lines are the fits of the spherical (S) and SCS models. Reproduced from Yokoyama *et al.*[21] with permission.

are square roots of 1, 3, 4 and 7 relative to the first-order peak position, which is an indication of a 2D hexagonal structure. In addition to these Bragg peaks, the circular patterns of the characteristic fringe are clearly observed in Figure 4a. The characteristic fringe is indicative of the form factor of the spherical nanocells. In the traditional transmission SAXS experiments in Figure 1, the form factor overlaps with the structure factor of the lattice; therefore, a quantitative analysis of the form factor to determine the shape of the nanocells is difficult.

However, aligning nanocells in a 2D hexagonal structure in a thin film effectively isolates the form factor of the domains from the structure factor of the lattice. The GISAXS intensity along the q_z axis on the first-order peak is plotted in Figure 4b. The two strong peaks in the low q_y region between 0.2 and 0.3 nm^{-1} are characteristic of the Yoneda wings from the critical angles of the nanocellular film and silicon substrate. As q_z increases, the intensity decays with small oscillations due to the interference between X-rays reflected from the surfaces of the nanocellular film and the silicon, and then it shows a distinct fringe. The fringe at a q_z of 0.53 nm^{-1} is part of the form factor that appeared as a ring pattern in Figure 4a because the nanocells are spherical objects. The structure factor of the lattice (the Bragg peaks) is completely eliminated in the z slice because the ordering of the nanocells is restricted to the plane of the film.

To analyze the GISAXS pattern quantitatively, a computation with a model using the distorted wave Born approximation (DWBA)[29,46,47] is necessary. The background of the DWBA and the model have been published previously.[21] First, we compare the z slice of the GISAXS pattern and the computed intensities using a spherical (S) model. The S model assumes an empty core surrounded by a uniform matrix and thus provides the following form factor, $F_S(q,R)$:

$$F_S(q,R) = \frac{3[\sin(qR) - qR\cos(qR)]}{(qR)^3},$$

where q and R are the wave vector and radius of the empty core, respectively. The S model does not fit all the data simultaneously, as indicated in Figure 4b, and hence, the form factor of a spherical empty core is not an appropriate model for the nanocells. From the proposed mechanism of nanocellular formation, CO_2 is introduced into the CO_2-philic domains; therefore, the empty cells are supposed to be surrounded by CO_2-philic domains, which are fluorine-containing PFMA block domains with a higher scattering density, in a matrix of non-CO_2-philic domains. To describe such a structure, the spherical concentric shell (SCS) model was introduced. The SCS model uses an empty core surrounded by a thin shell of CO_2-philic PFMA domains and a continuous non-CO_2-philic PS matrix. The form factor of the SCS model has been given by

$$F_{SCS}(q,\{R_k\}) = \frac{\rho_1 V(R_1) F_S(q,R_1) + \sum_{k=2}^{3} (\rho_k - \rho_{k-1}) V(R_k) F_S(q,R_k)}{\rho_1 V(R_1) + \sum_{k=2}^{3} (\rho_k - \rho_{k-1}) V(R_k)},$$

where ρ and V are the scattering density and volume, respectively. $\{R_k\}$ represents a set of radii to define the SCS model. The index k represents the media of regions 1, 2 and 3 corresponding to air, a CO_2-philic domain and a non-CO_2-philic domain, respectively. The SCS model provides a reasonable fit to the experimental data in all q_z ranges, as shown by a solid line in Figure 4b. This successful fit of the SCS model to the GISAXS profile is evidence of spherical nanocells, where CO_2 localizes in CO_2-philic domains and produces cells in each spherical domain of the CO_2-philic domains upon depressurization. The combination of thin film confinement to align ordered nanostructures and the use of GISAXS enables us to separate the form factor from the structure factor and to determine the detailed structure of the nanocells.

OPEN NANOPOROUS STRUCTURES TEMPLATED FROM BLOCK COPOLYMER MORPHOLOGIES

As previously presented, the CO_2 process with sphere-forming block copolymer templates successfully introduces nanocells into polymeric materials. CO_2 selectively swells CO_2-philic domains and introduces nanocells into the CO_2-philic domains. For this study, PS-PFMA, in which PFMA and PS blocks work as CO_2-philic and non-CO_2-philic blocks, respectively, was used. This methodology is not necessarily limited to spherical nanocells but can be extended to block copolymer templates with nonspherical domains. In this section, I show that selective swelling with CO_2 of block copolymer thin films induces morphological changes and results in unique nanosheet structures. In particular, the fabrication of horizontally or vertically stacked nanosheet structures of block copolymer bilayers on substrates will be discussed.

Two block copolymer thin films with cylindrical domains were prepared by spin-casting using two different solvents. While the natural morphology of the block copolymer is cylindrical, the selectivity of the solvent used for spin-casting influences the orientation of the cylindrical domains in thin films as reported previously.[22] One of these films has random orientation, and the other has perpendicular orientation. We used random orientation and perpendicular orientation films as templates to fabricate nanoporous thin films. The resultant nanoporous thin films were analyzed using GISAXS.

The random orientation film, with network-like domains without any preferential orientation before the process, was converted by the CO_2 process to a nanoporous film. The GISAXS patterns of the random orientation films in Figure 5a show irregularly spaced peaks along the q_z axis. To understand the GISAXS peak patterns, DWBA calculations are necessary to extract quantitative information; however, I will analyze the scattering pattern qualitatively using two sets of scattering events. The transmitted X-ray can be directly scattered and then transmitted through the sample, which is defined as a TT event. However, the X-ray can be reflected by the substrate, scattered and then transmitted through the sample, which is defined as a RT event. Due to these two scattering events, we found two sets of peaks in the GISAXS pattern. I only consider TT and RT of the four possible events in the DWBA.[29,46,47] These two scattering events can be separated because a TT event does not depend on the incident angle, while a RT event does depend on the incident angle because reflection is involved. While the set of TT peaks is stationary, the set of RT peaks shifts with increasing incident angle. Each set of peaks can be assigned to the ratios of 1, 2 and 3, respective to the first-order peak, and thus, the structure is a one dimensionally layered structure parallel to the surface. While a cylindrical nanoporous structure is expected from a cylinder-forming diblock copolymer, the resultant nanoporous structure was clearly stacked nanosheets separated from one another, and the stacking on the substrate is also supported by microscopy.[22]

It is possible that the nanosheet structures were templated from swollen lamellae in CO_2. During the CO_2 process, the cylindrical morphology of the block copolymer was converted to a lamellar morphology by selective swelling of the cylinder domains because cylindrical domains are CO_2-philic. Such selective swelling changes the effective volume fraction of the cylindrical domains and changes the cylinder domains to lamellar domains. In other words, an OOT was induced by selective swelling with CO_2. The evidence of an OOT

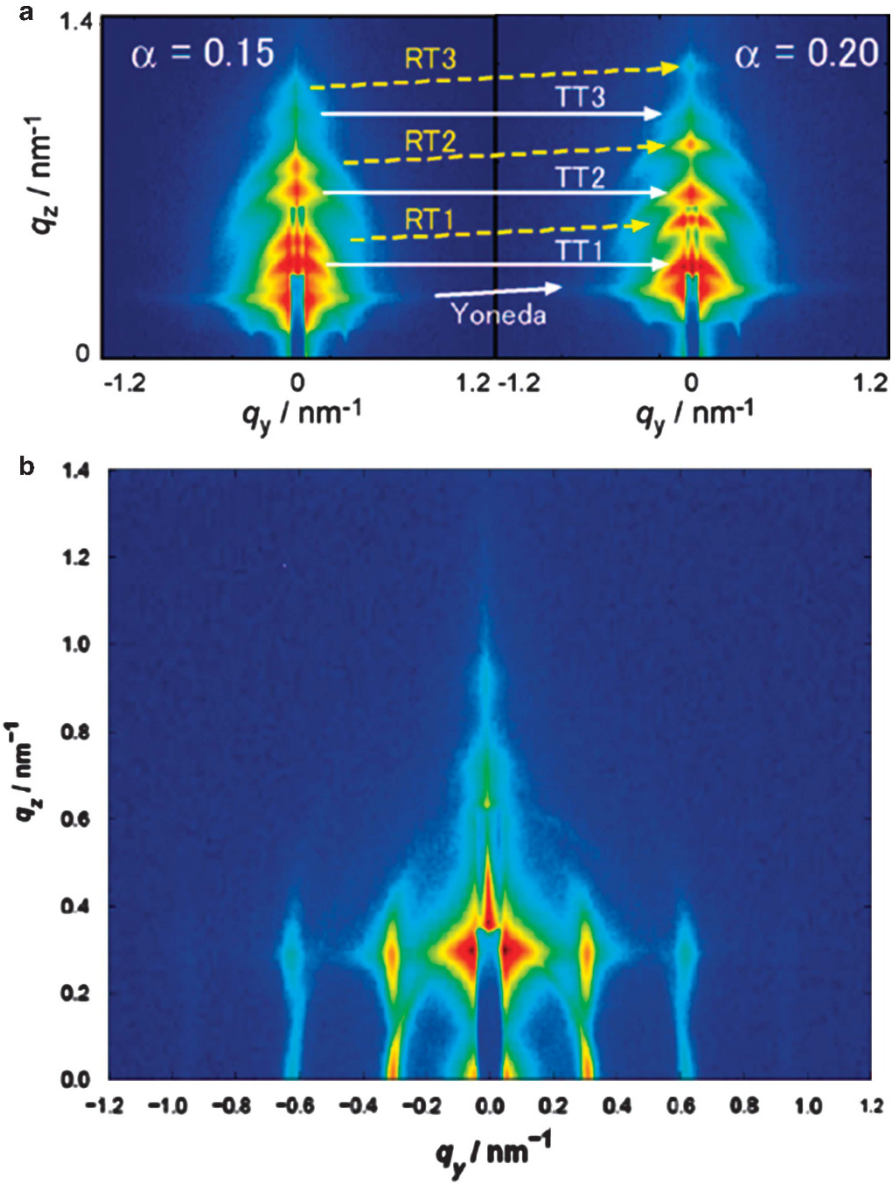

Figure 5 (**a**) GISAXS patterns of the random orientation films. q_y and q_z are the wave vectors parallel and perpendicular to the film plane, respectively. On the q_z axis, a rectangular beam-stop and attenuator are installed. T and R represent transmission and reflection components, respectively. For example, RT2 indicates the second order peak of the reflected, scattered and transmitted X-ray. Two different incident angles α of 0.15 (left) and 0.20 (right) degrees are compared. (**b**) GISAXS patterns of the perpendicular orientation films. Reproduced from Yokoyama *et al.*[22] with permission.

by selective swelling with CO_2 will be shown in the following section. Such parallel orientation of the lamellae, which were converted to nanosheets, has been widely observed when one component prefers to wet the surface or interface. The block copolymer used in our study contains a CO_2-philic block and hence prefers to cover the surface in CO_2.

As previously mentioned, perpendicular orientation films have cylindrical domains oriented perpendicular to the surface. Such films were similarly processed with CO_2 and analyzed using GISAXS. An example of GISAXS patterns of the perpendicular orientation films is shown in Figure 5b. The higher order peaks appear roughly at integer multiples of the first-order peak position in the q_y direction along the substrate. The expected structure is one dimensionally aligned nanosheets standing perpendicular to the surface and substrate. Such a finding of this structure is supported by microscopic observation.[22] However, as already mentioned, the block copolymer prefers a parallel orientation as the equilibrium structure to cover the surface with a CO_2-philic block. Therefore, the vertical orientation seems to be a metastable orientation induced by the pre-aligned cylindrical domains standing perpendicular to the surface. It is clearly indicated that lamellae, which were later converted to nanosheets, were formed by connecting neighboring cylinders and hence the lamellae were aligned perpendicular to the surface.

IN SITU SAXS STUDY OF OOTS IN SUPERCRITICAL CARBON DIOXIDE

In the previous sections, it was shown that fabricated porous structures were not always related to the original block copolymer

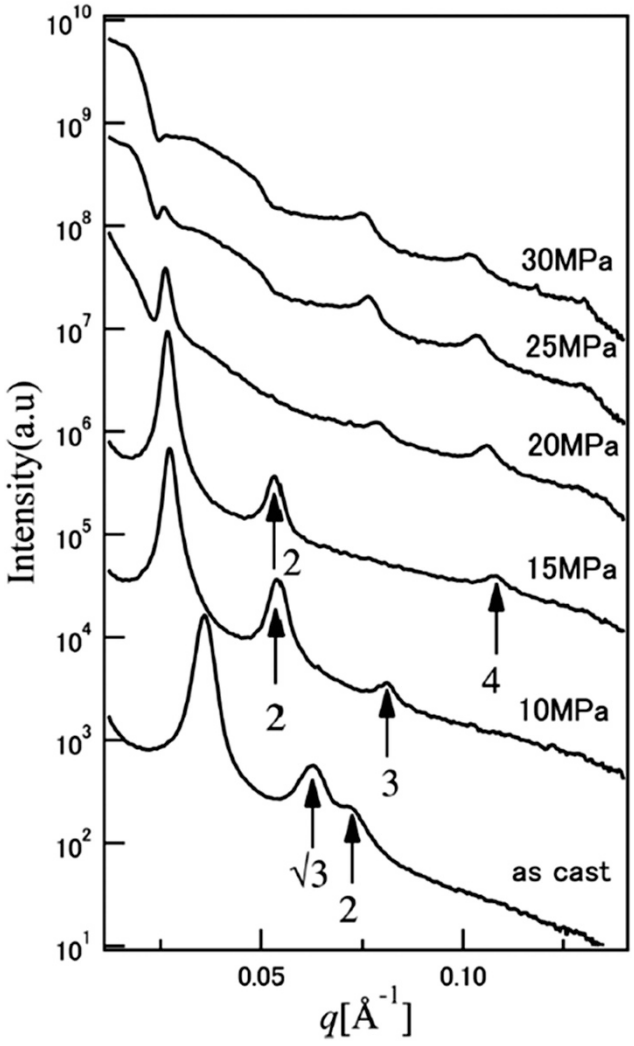

Figure 6 SAXS profiles of neat PS-PFMA at 60 °C as a function of the CO_2 pressure during pressurization. Above 10 MPa, all Bragg peak positions are located at integer multiples of the first-order peak position. Reproduced from Shinkai *et al.* [26] with permission.

morphologies, which suggested an OOT during the CO_2 process. In this section, an example of the observation of an OOT using *in situ* SAXS will be shown. The phase transition behavior of PS-PFMA in CO_2 was investigated using *in situ* SAXS. *In situ* SAXS experiments were performed on block copolymers swollen with CO_2 at 60 °C, well above the glass transition temperature of PS, in supercritical carbon dioxide (30 °C).[25] Figure 6 shows *in situ* SAXS profiles of PS-PFMA pressurized under CO_2 from the as-cast state up to 30 MPa at 60 °C. The as-cast sample clearly shows the Bragg peaks of a hexagonal phase, in which the peak ratios are 1: $3^{1/2}$: 2 relative to the first-order Bragg peak position. The domain spacing $d = 2\pi/q$ monotonically increases with increasing pressure. The peak ratio changed to 1: 2: 3 at 10 MPa, indicating an OOT from hexagonal cylinders to lamellae. This OOT is in good accord with the nanosheets obtained from the cylinder-forming diblock copolymer, as shown in the previous section. In the pressure range from 25 to 30 MPa, the structure factor disappeared and only the form factor was observed. This unknown structure with the form factor was identified to be a foam-like structure with bilayer walls of block copolymer chains after the sample was taken out from the CO_2 and observed by scanning electron microscopy. This finding indicated that a separation of bilayer sheets occurred in the swollen lamellae in CO_2. The wall thickness can be quantified from the form factor of the *in situ* SAXS profile and agrees very well with the expected bilayer thickness of the block copolymer chains. As we see here, a PS-PFMA block copolymer can be selectively swollen by CO_2 and exhibited an OOT. As well as the expected OOT from cylinders to lamellae, a unique transition to a foam-like structure was also seen. By using an *in situ* SAXS experiment, it can be clearly stated that the foam did not appear during a depressurization process but already existed in pressurized CO_2. The details of the OOT and other transitions are being investigated in our group by utilizing *in situ* SAXS.

CONCLUSIONS

A unique method for producing nanocells and nanopores using a block copolymer template with supercritical carbon dioxide was developed. Precise analysis of these nanoscale structures requires the use of SAXS. To overcome the well-known problem of interference between form and structure factors, thin-film confinement was used. In a thin film, for example, a single-layer thick film, the packing of domains is only restricted in the two-dimensional plane so that the form factor of a three-dimensional object can be isolated along the direction normal to the film. GISAXS was proven to be an effective method in studying such structures when combined with precise analysis using the DWBA. In addition, SAXS probed the swollen structure of block copolymers in supercritical carbon dioxide while the system was in high pressure supercritical CO_2 showed that an OOT occurred by selective swelling in CO_2, and the findings showed that the swollen structure was directly related to the obtained nanocellular and nanoporous structures.

CONFLICT OF INTEREST

The authors declare no conflict of interest.

ACKNOWLEDGEMENTS

This work has been financially supported by PRESTO-JST. The SAXS experiments reproduced here were performed at the Photon Factory with the approval numbers 2009G149 and 2011G168 and at the BL40B2 beamline at the SPring-8 synchrotron radiation facility.

1 Lee, S. B., Mitchell, D. T., Trofin, L., Nevanen, T. K., Soederlund, H. & Martin, C. R. Antibody-based bio-nanotube membranes for enantiomeric drug separations. *Science* **296,** 2198–2200 (2002).
2 Kohli, P., Harrell, C. C., Cao, Z. H., Gasparac, R., Tan, W. H. & Martin, C. R. DNA-functionalized nanotube membranes with single-base mismatch selectivity. *Science* **305,** 984–986 (2004).
3 Linssen, T., Cassiers, K., Cool, P. & Vansant, E. F. Mesoporous templated silicates: an overview of their synthesis, catalytic activation and evaluation of the stability. *Adv. Colloid Interface Sci* **103,** 121–147 (2003).
4 Lazzeri, P., Vanzetti, L., Anderle, M., Bersani, M., Park, J. J., Lin, Z., Briber, R. M., Rubloff, G. W., Kim, H. C. & Miller, R. D. Thin-film transformations and volatile products in the formation of nanoporous low-k polymethylsilsesquioxane-based dielectric. *J. Vac. Sci. Technol. B* **23,** 908–917 (2005).
5 Kresge, C. T., Leonowicz, M. E., Roth, W. J., Vartuli, J. C. & Beck, J. S. Ordered mesoporous molecular sieves synthesized by a liquid-crystal template mechanism. *Nature* **359,** 710–712 (1992).
6 Yang, P., Zhao, D., Margolese, D. I., Chmelka, B. F. & Stucky, G. D. Generalized syntheses of large-pore meosporous metal oxides with semicrystalline frameworks. *Nature* **396,** 152–155 (1998).
7 Yang, H., Coombs, N., Sokolov, I. & Ozin, G. A. Free-standing and oriented mesoporous silica films grown at the air–water interface. *Nature* **381,** 589–592 (1996).
8 Armatas, G. S. & Kanatzidis, M. G. Hexagonal mesoporous germanium. *Science* **313,** 817–820 (2006).
9 Inagaki, S., Guan, S., Ohsuna, T. & Terasaki, O. An ordered mesoporous organosilica hybrid material with a crystal-like wall structure. *Nature* **416,** 304–307 (2002).

10 Sun, D., Riley, A. E., Cadby, A. J., Richman, E. K., Korlann, S. D. & Tolbert, S. H. Hexagonal nanoporous germanium through surfactant-driven self-assembly of Zintl clusters. *Nature* **441,** 1126–1130 (2006).
11 Attard, G. S., Glyde, J. C. & Göltner, C. G. Liquid-crystalline phases as templates for the synthesis of mesoporous silica. *Nature* **378,** 366–368 (1995).
12 Lee, J. S., Hirao, A. & Nakahama, S. Polymerization of monomers containing functional silyl groups. 7. Porous membranes with controlled microstructures S. *Macromolecules* **22,** 2602–2606 (1989).
13 Zalusky, A. S., Olayo-Valles, R., Wolf, J. H. & Hillmyer, M. A. Ordered Nanoporous Polymers from Polystyrene−Polylactide Block Copolymers. *J. Am. Chem. Soc* **124,** 12761–12773 (2002).
14 Thurn-Albrecht, Steiner, T. R., Derouchey, J., Stafford, C. M., Huang, E., Bal, M., Tuominen, M., Hawker, C. J. & Russell, T. P. Nanoscopic Templates from Oriented Block Copolymer Films. *Adv. Mater* **12,** 787–791 (2000).
15 Chan, V. Z. H., Hoffman, J., Lee, V. Y., Iatrou, H., Avgeropolulos, A., Hadjichristidis, N., Miller, R. D. & Thomas, E. L. Ordered bicontinuous nanoporous and nanorelief ceramic films from self assembling polymer precursors. *Science* **286,** 1716–1719 (1999).
16 Hashimoto, T., Tsutsumi, K. & Funaki, Y. Nanoprocessing based on bicontinuous microdomains of block copolymers: nanochannels coated with metals. *Langmuir* **13,** 6869–6872 (1997).
17 Li, L., Yokoyama, H., Nemoto, T. & Sugiyama, K. Facile fabrication of nanocellular block copolymer thin films using supercritical carbon dioxide. *Adv. Mater* **16,** 1226–1229 (2004).
18 Li, L., Nemoto, T., Sugiyama, K. & Yokoyama, H. CO2 foaming in thin films of block copolymer containing fluorinated blocks. *Macromolecules* **39,** 4746–4755 (2006).
19 Yokoyama, H., Li, L., Nemoto, T. & Sugiyama, K. Tunable nanocellular polymeric monoliths using fluorinated block copolymer templates and supercritical carbon dioxide. *Adv. Mater* **16,** 1542–1546 (2004).
20 Yokoyama, H. & Sugiyama, K. Nanocellular structures in block copolymers with CO2-philic blocks using CO2 as a blowing agent: Crossover from micro- to nano-cellular structures with depressurization temperature. *Macromolecules* **38,** 10516–10522 (2005).
21 Yokoyama, H., Dutriez, C., Li, L., Nemoto, T., Sugiyama, K., Sasaki, S., Masunaga, H., Takata, M. & Okuda, H. Grazing incident small angle X-ray scattering study of polymer thin films with embedded ordered nanometer cells. *J. Chem. Phys* **127,** 014904 (2007).
22 Yokoyama, H., Li, L., Dutriez, C., Iwakura, Y., Sugiyama, K., Masunaga, H., Sasaki, S. & Okuda, H. Horizontally and vertically aligned polymeric nanosheets: CO2-induced morphological transition of block copolymer templates. *Macromolecules* **41,** 8626–8631 (2008).
23 Zhang, R. & Yokoyama, H. Fabrication of nanoporous structures in block copolymer using selective solvent assisted with compressed carbon dioxide. *Macromolecules* **42,** 3559–3564 (2009).
24 Zhang, R., Dutriez, C., Sugiyama, K., Ishizone, T. & Yokoyama, H. Thermally robust nanocellular thin films of high-Tg semifluorinated block copolymers foamed with supercritical carbon dioxide. *Soft Matter* **7,** 4032–4038 (2011).
25 Dutriez, C., Satoh, K., Kamigaito, M. & Yokoyama, H. Nanocellular foaming of fluorine containing block copolymers in carbon dioxide: the role of glass transition in carbon dioxide. *RSC Adv* **2,** 2821–2827 (2012).
26 Shinkai, T., Ito, M., Sugiyama, K., Ito, K. & Yokoyama, H. Ordered and foam structures of semifluorinated block copolymers in supercritical carbon dioxide. *Soft Matter* **8,** 5811–5817 (2012).
27 Dutriez, C., Satoh, K., Kamigaito, M. & Yokoyama, H. Nanometer voids prevent crack growth in polymeric materials. *Macromolecules* **40,** 7433–7436 (2007).
28 Mahltig, B., Muller-Buschbaum, P., Wolkenhauer, M., Wunnicke, O., Wiegand, S., Gohy, J. F., Jerome, R. & Stamm, M. J. Highly Regular Polyampholytic Structures Adsorbed Directly from Solution. *Colloid Interface Sci* **242,** 36 (2001).
29 Lazzari, R. IsGISAXS a program for grazing-incidence small-angle X-ray scattering analysis of supported islands. *J. Appl. Crystallogr* **35,** 406 (2002).
30 Muller-Buschbaum, P. Grazing incidence small-angle X-ray scattering: an advanced scattering technique for the investigation of nanostructured polymer films. *Anal. Bioanal. Chem* **376,** 3 (2003).
31 Gibaud, A., Baptiste, A., Doshi, D. A., Brinker, C. J., Yang, L. & Ocko, B. Wall thickness and core radius determination in surfactant templated silica thin films using GISAXS and X-ray reflectivity. *Europhys. Lett* **63,** 833 (2003).
32 Gibaud, A., Grosso, D., Smarsly, B., Baptiste, A., Bardeau, J. F., Babonneau, F., Doshi, D. A., Chen, Z., Brinker, C. J. & Sanchez, C. Evaporation-Controlled Self-Assembly of Silica Surfactant Mesophases. *J. Phys. Chem. B* **107,** 6114 (2003).
33 Gibaud, A., Dourdain, S., Gang, O. & Ocko, B. M. In situ grazing incidence small-angle x-ray scattering real-time monitoring of the role of humidity during the structural formation of templated silica thin films. *Phys. Rev. B* **70,** 161403 (2004).
34 Xu, T., Goldbach, J. T., Misner, M. J., Kim, S., Gibaud, A., Gang, O., Ocko, B., Guarini, K. W., Black, C. T., Hawker, C. J. & Russell, T. P. Scattering study on the selective solvent swelling inducing surface reconstruction. *Macromolecules* **37,** 2972–2977 (2004).
35 Park, I., Lee, B., Ryu, J., Im, K., Yoon, J., Ree, M. & Chang, T. Epitaxial phase transition of polystyrene-b-polyisoprene from hexagonally perforated layer to gyroid phase in thin film. *Macromolecule* **38,** 10532 (2005).
36 Lee, B., Oh, W., Hwang, Y., Park, Y. H., Yoon, J., Jin, K. S., Heo, K., Kim, J., Kim, K. W. & Ree, M. Imprinting well-controlled nanopores in organosilicate dielectric films: e-caprolactone and its chemical triethoxysilyl-modified six-armed poly(hybridization with organosilicate precursor. *Adv. Mater.* **17,** 696 (2005).
37 Lee, B., Park, I., Yoon, J., Park, S., Kim, J., Kim, K. W., Chang, T. & Ree, M. Scattering studies of nanoporous organosilicate thin films imprinted with reactive star porogens. *Macromolecules* **38,** 4311 (2005).
38 Lee, B., Oh, W., Yoon, J., Hwang, Y., Kim, J., Landes, B. G., Quintana, J. P. & Ree, M. Scattering studies of nanoporous organosilicate thin films imprinted with reactive star porogens. *Macromolecules* **38,** 8991 (2005).
39 Lee, B., Yoon, J., Oh, W., Hwang, Y., Heo, K., Jin, K. S., Kim, J., Kim, K. W. & Ree, M. n-Situ grazing incidence small-angle x-ray scattering studies on nanopore evolution in low-k organosilicate dielectric thin films M. *Macromolecules* **38,** 3395 (2005).
40 Sun, Z., Wolkenhauer, M., Bumbu, G. G., Kim, D. H. & Gutmann, J. S. GISAXS investigation of TiO2 nanoparticles in PS-b-PEO block-copolymer films. *Physica B* **357,** 141 (2005).
41 Gibaud, A., Dourdain, S. & Vignaud, G. Analysis of mesoporous thin films by X-ray reflectivity, optical reflectivity and grazing incidence small angle X-ray scattering. *Appl. Surf. Sci* **253,** 3 (2006).
42 Lee, B. D., Park, Y. H., Hwang, Y. T., Oh, W., Yoon, J. & Ree, M. Ultralow-k nanoporous organosilicate dielectric films imprinted with dendritic spheres. *Nat. Mater* **4,** 147 (2005).
43 Yoon, J., Yang, S. Y., Heo, K., Lee, B., Joo, W., Kim, J. K. & Ree, M. Nondestructive, quantitative synchrotron grazing incidence x-ray scattering analysis of cylindrical nanostructures in supported thin films M. *J. Appl. Crystallogr* **40,** 305 (2007).
44 Heo, K., Oh, K. S., Yoon, J., Jin, K. S., Jin, S., Choi, C. K. & Ree, M. Synchrotron x-ray scattering and reflectivity studies of the structure of low dielectric constant sioch thin films prepared from bistrimethylsilylmethane by chemical vapor deposition M. *J. Appl. Crystallogr* **40,** s614 (2007).
45 Yoon, J., Choi, S., Jin, S., Jin, K. S., Heo, K. & Ree, M. Quantitative analysis of molecularly stacked layer structure in supported organic thin films by synchrotron grazing incidence x-ray scattering. *J. Appl. Crystallogr* **40,** s669 (2007).
46 Sinha, S. K., Sirota, E. B., Garoff, S. & Stanley, H. B. X-ray and neutron scattering from rough surfaces. *Phys. Rev. B* **38,** 2297–2311 (1988).
47 Rauscher, M., Salditt, T. & Spohn, H. Small-angle X-ray scattering under grazing incidence: the cross section in the distorted-wave Born approximation. *Phys. Rev. B* **52,** 16855–16863 (1995).